Preprints (www.preprints.org) | NOT PEER-REVIEWED | Posted: 17 May 2021 doi:10.20944/preprints202105.0374.v1

Article

Change Mechanism of Strength of Soil-rock Mixture Freezing-thawing Interface under Different Rock

Gang Li , Tao Huang , Zhen Li , and Miaomiao Bai

School of Architecture and Civil Engineering, Xi'an University of Science and Technology, Xi'an 710054, China; 352339984@qq.com (T.H) 862038940@qq.com (Z.L) 997065015@qq.com (M.B)

* Correspondence: lg_gang_li@163.com or 19204209051@stu.xust.edu.cn

Abstract: With global warming and accelerated degradation of permafrost, the engineering problems caused by the formation of weak zones between the shallow and permafrost layers of soil–rock mixture (S-RM) slopes in permafrost regions have become increasingly prominent. To explore the influence of rock content on the shear strength of the S-RM freezing–thawing interface, the variation in the shear strength for different rock content is studied herein using direct shear tests. In addition, a 3D laser scanner is used for obtaining the topography of the shear failure surface. Combined with the analysis results of the shear band-particle calculation model, the influence of the rock content on the shear strength of the interface is explored. It was found that the impact threshold of the rock content on the interface strength and failure mode is approximately 30%, when the rock content (R) is > 30% and that the shear strength increases rapidly with increasing rock content. When R ≤ 30%, the actual shear plane is similar to waves; when R > 30%, the shear plane appears as gnawing failure. The shear strength of S-RM freezing–thawing interface mainly comes from the bite force and friction between particles. The main reason for the increase in shear strength with increasing rock content is the increase in bite force between particles, which makes the ratio of bite force to friction force approximately 1:1.

Keywords: soil–rock mixture, freezing–thawing interface, shear strength, shear failure surface, particle calculation model

1. Introduction

Soil-rock mixture (S-RM) is a loose geological material comprising engineering-scale block stone and fine-grained soil [1-3]. Different from the traditional homogeneous soil and cataclastic rock mass, its internal structure presents typical characteristics of heterogeneity, discontinuity, large pores, and multiple interfaces. Under the freezing condition, ice crystals fill the S-RM pores and provide adequate freezing force and the strength of S-RM increases significantly. Upon thermal thawing, the freezing force disappears and the internal skeleton gets restructured under the action of its own weight and load, decreasing the strength drastically. This shows the strong environmental dependence and susceptibility of S-RM. Moreover, their engineering property is extremely unstable. Due to global warming and accelerated degradation of permafrost, various types of slope instability in the Qinghai-Tibet Plateau frequently occur [4-7]. The active layer in the permafrost region often contains abundant ice crystals; when the slope melts from the surface to the inside, the ice crystals gradually melt into pore water. Because the frozen soil underneath the freezing front is impermeable, the melting S-RM active layer usually has high water content. When the active layer of the frozen soil slope begins to melt, a special freezing–thawing interface is formed [8]. S-RM in permafrost regions has complex physical and mechanical properties due to negative temperature and the presence of gravels [9-11]; this leads to increased water adsorption and infiltration retention in ice-rich layer, forming weak surfaces with soft upper and lower hard layers between shallow active and permafrost layers. The interface is rich in ice and has a low friction coefficient and often becomes the source of slope disasters in cold regions [12]. Therefore, it is necessary to

© 2021 by the author(s). Distributed under a Creative Commons CC BY license.

Preprints (www.preprints.org) | NOT PEER-REVIEWED | Posted: 17 May 2021 doi:10.20944/preprints202105.0374.v1

study the shear mechanical properties of S-RM freezing–thawing interface with different rock content.

S-RM is also known as bimrock or bimoil [13-15]. The shear properties of S-RM with different rock content have been studied extensively. Vallejo et al. [16] studied the influence of rock content in S-RM on the shear strength and void ratio. Simon and Houlsby [17] established a prediction formula for the shear strength of S-RM with a rock content of 0%–50% through large-scale direct shear test. Xu et al. [18] conducted large-scale direct shear tests on S-RM with a rock content of 0%–70% and found that the thickness of shear band and the internal friction angle increased with increasing rock content, while the cohesion decreased slightly. Through in situ direct shear test, Coli et al. [19] found that the internal friction angle of bimrock has a linear positive correlation with the rock content; the cohesion first increases and then decreases with increasing rock content, and a threshold value for cohesion is observed when the rock content is 20%–25%. Wei et al. [20] conducted direct shear tests on S-RM with different rock content and considered the impact of rock fragmentation; they found that the stress–strain curve showed a strain-hardening trend with increasing rock content, and particle breakage became more serious with increasing rock content, resulting in a power-law relationship between shear strength and normal stress.

As a weak zone in practical engineering, freezing–thawing interface has attracted increasing attention. Through field exploration and research, Mcroberts et al. [21] postulated that thawing plays a critical role in the failure of freezing–thawing interface of various landslides. Niu et al. [22] analyzed the stability of high-ice-content frozen soil on underground ice surfaces (freezing–thawing interface) by studying thermal thaw slumping in Qinghai–Tibet permafrost regions and proposed measures of waterproof and drainage to protect frozen soil. Through field and laboratory tests, Toloukian et al. [23] found that the shear strength at the freezing–thawing interface is greater than that of the thawed soil. Niu et al. [6] studied low-angle landslides in Qinghai–Tibet permafrost regions and found that the stagnant water lubrication effect at the freezing–thawing interface is one of the important reasons for slope instability. Shi et al. [24] used a direct shear instrument with a temperature control system to study the shear characteristics of the clay–ice interface and found that the initial water content and temperature determine the shear stress properties and dilatancy types of the interface. Ice bonds in frozen soil combine solid particles together, change the interaction between soil components and have a great impact on the mechanical behavior of soil. Internal temperature, humidity, and stress of frozen soil affect one another [25-27]. De Guzman et al. [28] found that in a certain temperature range, the strength of shear failure surface is positively proportional to negative temperature. Some researchers made freezing–thawing interface samples on the basis of the different freezing points of salt water and pure water and verified the failure mode of soil slope on the interface [29-30].

S-RM is widely distributed over the entire permafrost or periglacial region, and it is widely used in engineering. However, most of the previous studies have focused on the shear strength of S-RM in nonfrozen regions or have considered only the shear strength of the soil freezing–thawing interface. Basic research on shear weak zone of slope in frozen regions is insufficient, and there is little in-depth research on S-RM freezing–thawing interface. In the present study, considering that the freezing point of brine is lower than that of water, S-RM samples with freezing–thawing interface were prepared using brine and pure water. Based on the actual engineering background, direct shear tests of S-RM freezing–thawing interface with six different rock content (0, 10%, 20%, 30%, 35%, and 40%) under a high water content of 30% were conducted, and the shear strength parameters were obtained. The shear failure characteristics were obtained using 3D laser scanning. Combined with S-RM shear calculation model, the influence mechanism of rock content on shear strength of the interface was analyzed.

Preprints (www.preprints.org) | NOT PEER-REVIEWED | Posted: 17 May 2021 doi:10.20944/preprints202105.0374.v1

2. Test design

2.1. Sample preparation

From the field investigation of permafrost at the Fenghuoshan site of Golmud–Lhasa section where the reconstruction and expansion project of Qinghai–Tibet railway is underway, it was found that the permafrost in the crossing layer is gravel soil, mainly comprising angular (round) gravel and silty clay, with rock content of 10%–45%. The results show that the water content of the sliding mass in the melting season has reached the liquid limit of silty clay. The liquid limit and plastic limit of the fine-grained soil are 31.87% and 14.57%, respectively. Therefore, the representative values of fine-grained soil with controlled water content of 30% and rock content of 0%, 10%, 20%, 30%, 35%, and 40% were selected to make the remolded cylinder sample with the size of φ150 mm × 100 mm. The typical soil in Qinghai–Tibet permafrost region–silty clay, gravel, saline water, and pure water, were the main materials of this test. The grading curve of soil and gravel particles in the sample is shown in Figure 1. According to the standard for the particle size threshold of soil and rock: $d_{thr} = 0.05L_c$ [14,31], 5 mm is defined as the particle size limit between soil and rock in this test. According to the standard for geotechnical test methods (GB/T 50123-2019, 2019) [32], the maximum particle size of the gravel must not exceed 1/4 of the sample height and 1/8 of the sample diameter. Therefore, the maximum particle size of the gravels used in this test did not exceed 20 mm, and a suitable replacement method was used to remove oversized gravels.

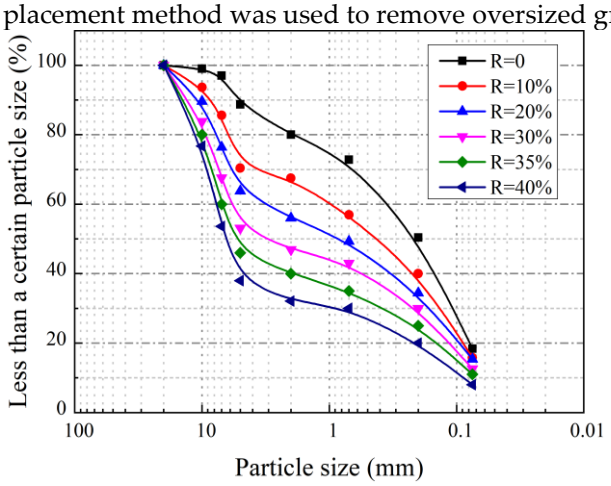

Figure 1. Gradation cumulative curve of soil-rock mixture.

During the sample preparation process, the fine-grained soil was first dried in a drying box at 110 °C for 24 h, crushed, and passed through a 2-mm sieve. Water was evenly sprayed on the surface of dry soil; the soil sample was then seal and covered with plastic film for 8 h to let the water infiltrate naturally. The density of the remolded sample was set at 2.0 g/cm^3, and the mass of clay and gravel was calculated according to the gradation curve. Clay and gravel mixed evenly and then compacted in three layers. The composite sample was made based on the characteristic that the freezing point of brine is lower than that of pure water. In the process of sample preparation, the corresponding parts of pure water and brine configuration were operated separately and there was no cross contact between them before combining. The sample preparation process was completed in 1–2 min. Next, the prepared sample were immediately placed in a low-temperature environment box for freezing. In the low-temperature environment, the exchange of water molecules became slow, ensuring that the freezing–thawing interface was not affected by temperature and that the moisture migration did not cause obvious retreat phenomenon of the freezing–thawing interface.

2.2. Test process

First, the composite sample with 1:1 volume ratio of 1.5% salt water with 30% water content in the upper layer soil and 18% pure water content in the lower layer soil was

Preprints (www.preprints.org) | NOT PEER-REVIEWED | Posted: 17 May 2021 doi:10.20944/preprints202105.0374.v1

made. The freezing temperature of salt water is approximately −5 °C, and the freezing temperature of pure water is approximately 0 °C. The samples were placed in an low-temperature environment box at −3 °C for 48 h. After freezing, the upper soil was in the thawing state at −3 °C while the lower soil was in the freezing state so that the upper part was thawed soil and the lower part was frozen soil, and there was a freezing–thawing interface in the middle. Then, the improved strain-controlled direct shear instrument was used to carry out the low temperature direct shear test of the freezing–thawing interface. A low-temperature laboratory developed by Xi'an University of Science and Technology served as the test environment, and the indoor temperature was set as approximately −3 °C. The shear rate was 0.8 mm/min. During the test process, the data were recorded using the automatic data acquisition instrument and inputted into the computer for real-time reading and recording. After the sample was sheared, to obtain the 3D shape of the shear plane, a 3D laser scanner was used to measure the distance of the shear plane point by point, and then the relative elevation Z of each measuring point was obtained by conversion. Then, the 3D coordinates (x, y, z) of each measuring point were obtained, the test process is shown in Figure 2.

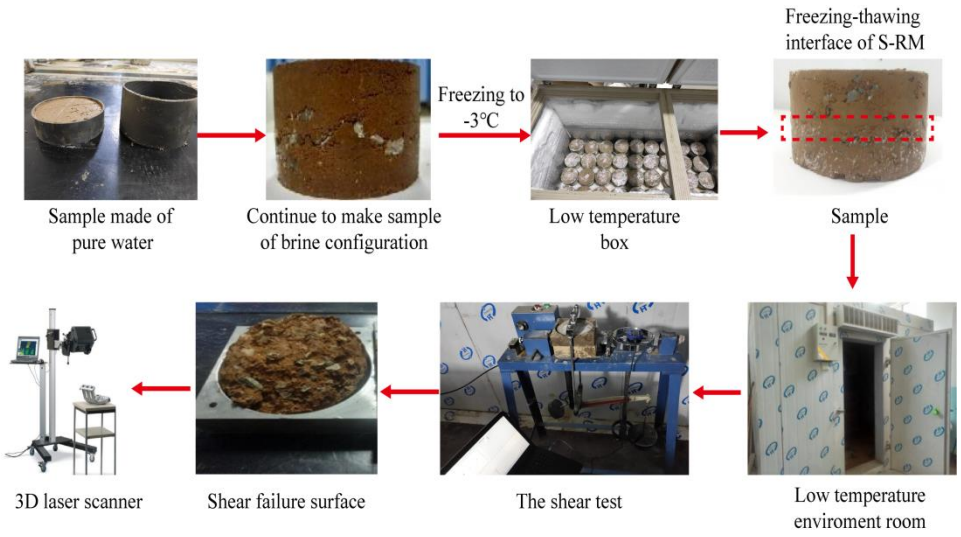

Figure 2. Test process.

According to the field investigation, the freezing–thawing interface of S-RM slope is observed mostly at a depth of approximately 0.5–3 m in the shallow layer. Four normal stresses of 50, 100, 200, and 300 kPa were selected in the test. Because the shear position of the interface was fixed artificially, the shear occurred at the interface between thawed soil and frozen soil. The specific conditions were grouped as shown in Table 1. Three parallel tests were conducted for each condition.

Table 1. Test conditions.

Water content/%	Rock content/%	Normal stress/kPa
30	0	50, 100, 200, 300
	10	50, 100, 200, 300
	20	50, 100, 200, 300
	30	50, 100, 200, 300
	35	50, 100, 200, 300
	40	50, 100, 200, 300

3. Test results

3.1. Stress–strain relationship

Preprints (www.preprints.org) | NOT PEER-REVIEWED | Posted: 17 May 2021 doi:10.20944/preprints202105.0374.v1

As an important characteristic of S-RM, rock content largely determines its mechanical properties and deformation failure mode. Through the direct shear test, the stress–strain curves of S-RM freezing–thawing interface with different rock content under different normal stresses were obtained (Figure 3). Under different normal stresses, the stress–strain curves of R = 0 and R = 10% basically coincide; the shape and position of the stress–strain curves for R ≤ 30% and R > 30% are obviously different. The slope of the linear elastic phase of the stress–strain curve increases with increasing rock content; this is closely related to the occlusion of gravel in the shear band. When the normal stress is 50 and 100 kPa, the stress–strain curves for R ≤ 30% are of the strain-hardening type; when R > 30%, the stress–strain curves show the characteristics of strain softening. With increasing rock content, the stress–strain curve changes from strain hardening to strain softening. When the normal stress is 200 and 300 kPa, the stress–strain curves show the characteristics of strain hardening and zigzag, accompanied by intermittent jumping in the process of climbing. This jumping growth is closely related to the occlusion and overturning of rock particles in the shear band.

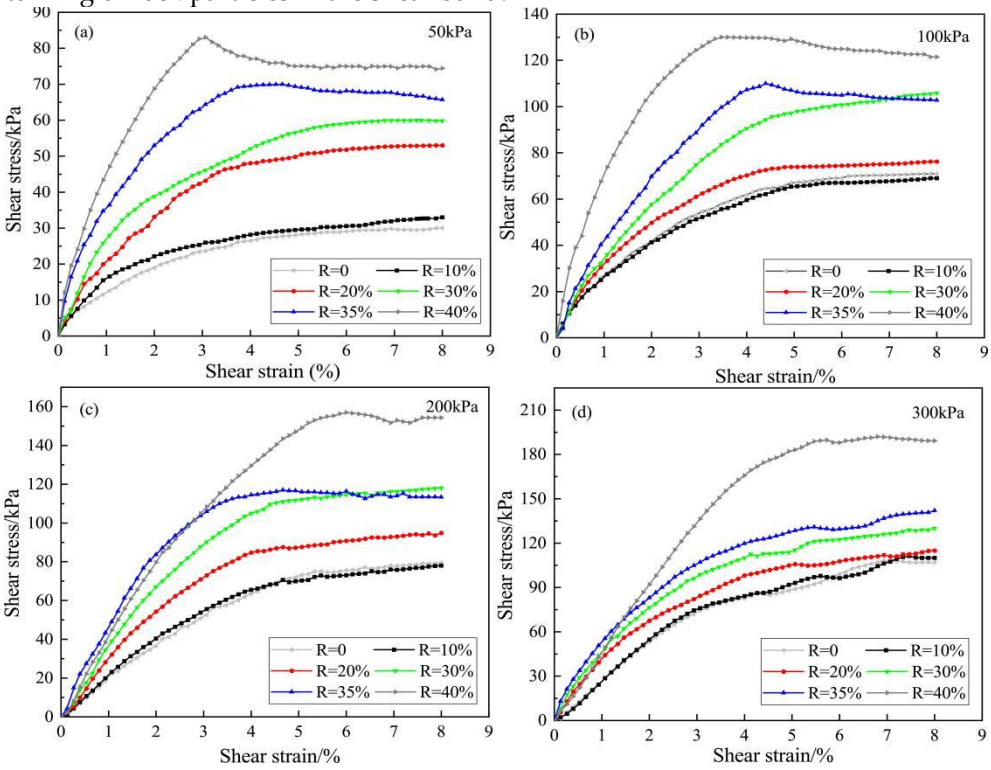

Figure 3. Stress–strain curves of the samples with different rock content under different normal stresses: (a) 50kPa; (b) 100kPa; (c) 200kPa; (d) 300kPa.

3.2. Shear strength parameters

The changes in the shear strength of the freezing–thawing interface under different rock content are shown in Figure 4. With increasing rock content, the shear strength of the freezing–thawing interface gradually increased. When the rock content increased from 0% to 10%, the shear strength did not increase significantly. This is because when the rock content is 10%, there are fewer rock particles distributed near the freezing–thawing interface, which cannot provide stable embedding during the shearing process. With increasing rock content, the number of rock particles near the freezing–thawing interface increased and the rolling of gravels in the frozen and thawing soil layers was restricted by each other's embedment and resistance, which led to the increase in the shear strength of the interface. Based on the growth rate of the shear strength under different rock content, 30% rock content is the threshold value and the change in the shear strength with rock content is divided into two stages. When R ≦ 30% (stage 1), the interface shear strength increases slowly with increasing rock content. When R > 30% (stage 2), the shear strength growth rate of the interface increases significantly; in this case, the

Preprints (www.preprints.org) | NOT PEER-REVIEWED | Posted: 17 May 2021 doi:10.20944/preprints202105.0374.v1

soil and rock particles are closely connected and the occlusion between particles near the shear band is enhanced.

The shear strength of the interface increased with increasing normal stress. The main reason is that the increase in normal stress leads to increase of compactness of the sample, improving the bite force between particles, and the Poisson effect of S-RM is prominent.

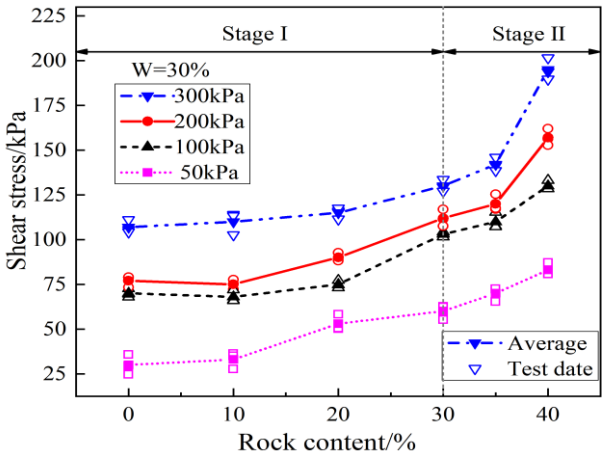

Figure 4. Variation in the shear strength of the samples with different rock content.

From Table 2, it can be seen that the growth rate of shear strength with increasing rock content under different normal stresses is different. When R = 10%, 20%, and 35%, the growth rate of shear strength under low normal stress (50 kPa) is greater than that under medium and high normal stress. When R = 30%, the change rate of shear strength under medium normal stress (100 and 200 kPa) is the most obvious. When R = 40%, the shear strength increases most significantly under high normal stress (300 kPa).

Table 2. Increment rate of shear strength at different rock content

Rock content (%)	Shear strength's increment rate (%)			
	50 (kPa)	100 (kPa)	200 (kPa)	300 (kPa)
10	10.05	-2.86	-2.60	2.80
20	60.61	10.29	20.08	4.54
30	13.21	37.33	24.44	13.04
35	16.67	6.80	7.14	9.23
40	18.57	18.18	30.83	37.32

Based on the results of Figure 4, the variation in cohesion and internal friction angle with increasing rock content is obtained using the Mohr-Coulomb criterion (Figure 5). With increasing rock content, the cohesion first decreases and then increases, reaching the minimum value when the rock content is 10%, and then presents a linear increase. When the rock content is 10%, the cohesion decreases because the blocks are in a suspended state inside the S-RM, which does not have a positive effect on cementation between the particles. Simultaneously, the presence of rock particles prevents contact between soil particles, thereby decreasing cohesion. Subsequently, due to the presence of more number of rock particles, the clay particles squeeze and bond with each other during the shearing process and show a linear increase with increasing rock content. The internal friction angle increases with increasing rock content, increasing significantly when the rock content reaches 35%. This significant increase is closely related to the internal structure of the sample. When the rock content reaches 35%, the skeleton effect of the sample is prominent, and the bite force between the rocks increases greatly. Moreover, more gravel embedded in the lower frozen soil layer provides greater resistance, which eventually increases the bite force between the particles at the interface.

Preprints (www.preprints.org) | NOT PEER-REVIEWED | Posted: 17 May 2021 doi:10.20944/preprints202105.0374.v1

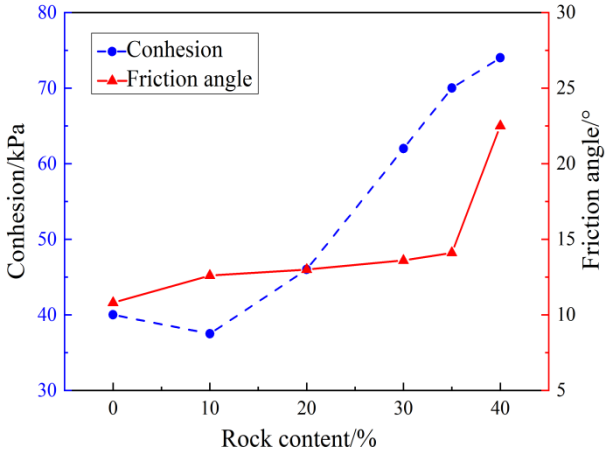

Figure 5. Variation regularity of shear strength parameters with different rock content.

The ratio of cohesion and internal friction angle of S-RM freezing–thawing interface to parameters of pure soil freezing-thawing interface under different rock content is shown in Table 3. When the rock content increases from 0% to 10%, the change in internal friction angle is obvious. When the rock content increases from 20% to 35%, the influence of gravel on the change of cohesion is greater. When the rock content reaches 40%, the skeleton effect between gravel is enhanced, leading to a more obvious change in the internal friction angle.

Table 3. Ratio of shear strength parameters to initial parameters with different rock content.

Strength index	Rock content/%				
	10	20	30	35	40
c	0.94	1.15	1.55	1.75	1.85
φ	1.17	1.20	1.26	1.31	2.08

3.3. 3D morphology of shear plane

Because the failure must produce strength, there must be a relationship between shear strength and failure characteristics. Therefore, to analyze the mechanism of S-RM freezing–thawing interface strength, it is necessary to explore the shear surface morphology. After shearing, the upper shear box was lifted away, and then the lower shear plane was scanned point by point using a 3D scanner. The distance between each scanning point on the shear plane and the laser rangefinder obtained via scanning was stored in an Excel file. Then, Sufer software was used to read the data and to draw the 3D morphology of S-RM interface after shear failure, as shown in Figure 6 (normal stress of 100 kPa). When R ≤ 30%, the shear failure surface exhibited wavy failure with small fluctuations and the surface was relatively uniform. When R > 30%, the shear failure surface exhibited gnawing failure with obvious fluctuations and the surface was nonuniform.

Preprints (www.preprints.org) | NOT PEER-REVIEWED | Posted: 17 May 2021 doi:10.20944/preprints202105.0374.v1

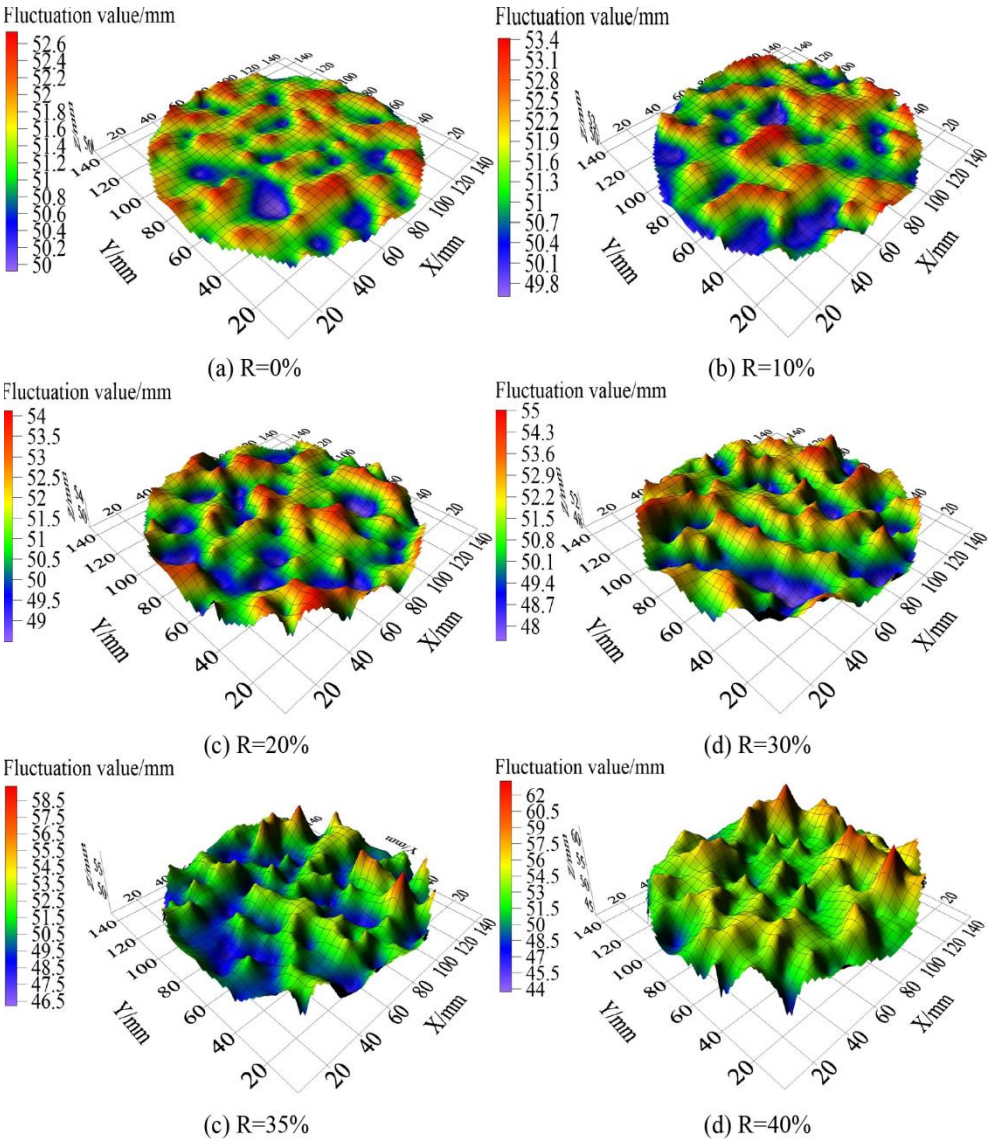

Figure 6. 3D topography of shear failure surface under different rock content: (a) R=0%;

(b) R=10%; (c)R=20%; (d) R=30%; (e) R=35%; (f) R=40%.

From Figure 7, it can be seen that the undulation value of the shear failure surface of the sample gradually increases with increasing rock content. Similar to the law of shear strength variation, the increasing trend of fluctuation value has a threshold at R = 30%. When R ≤ 30%, the undulation value of the shear surface undergoes a small change, the rock content increases from 0% to 30%, the undulation value increases from 2.8 to 7.2 mm, and the undulation value of R = 30% is 2.6 times that of R = 0. When R > 30%, the undulation value of shear surface increases obviously. When R = 35%, the undulation value is 12.4 mm, and when R = 40%, the undulation value is 19 mm, which are 4.4 and 6.8 times the undulation value when R = 0, respectively.

Preprints (www.preprints.org) | NOT PEER-REVIEWED | Posted: 17 May 2021 doi:10.20944/preprints202105.0374.v1

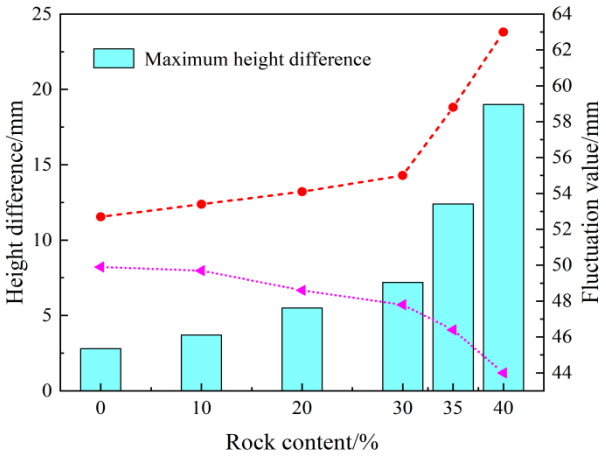

Figure 7. Fluctuation value of the shear surface of the samples with different rock content.

4. Discussion

4.1. Establishment and analysis of shear strength calculation model of the interface

During the shearing process, particles near the freezing–thawing interface bite, overturn, and rub against each other, and the sharp corners of gravels are sheared when normal stress is large, which are the reasons for the shear strength. Therefore, the shear strength of S-RM freezing–thawing interface is mainly composed of bite force, friction force, and crushing force between particles, while the crushing force itself contributes little to the shear strength and the working condition studied in this paper is the case of low normal stress, so the influence of crushing force is not considered here.

Based on previous research [33], the irregular particles in the shear band are simplified as ellipses, and the shear strength calculation model is established, as shown in Figure 8. Under the action of constant normal pressure N and shear force T, particles in the shear band tumble and rub. The length of the long half axis of elliptical particles is a, and the length of the short half axis is b. It is assumed that the rotation angle of the particles moving from point A to B is 90°. Suppose the angle between the contact surface and horizontal plane when sliding to any position is α, let α_0 be the angle at the initial position (at point A), and let θ be the angle between the line connecting the tangent point and the center of the circle and X-axis when sliding to any position.

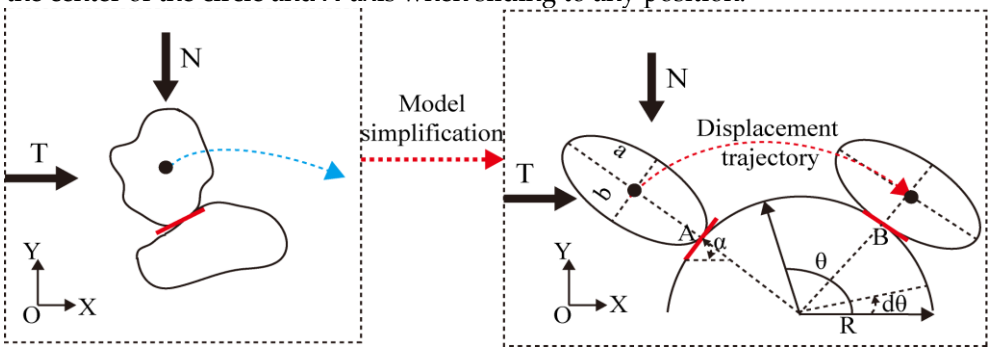

Figure 8. Calculation model of particle shear strength in shear band.

The contribution of bite force in the shearing process is divided into angular rotation work and displacement work. The angular rotation work can be expressed as

$$W_\theta = \int_{\frac{\pi}{2}+\alpha_0}^{\frac{\pi}{2}-\alpha_0} \Delta I a d\theta \quad (1)$$

w

Preprints (www.preprints.org) | NOT PEER-REVIEWED | Posted: 17 May 2021 doi:10.20944/preprints202105.0374.v1

here dθ is the increment of angular rotation, and ΔI is the component of shear force to rotation.

$$\Delta I = N\cos\alpha\cos\varphi_{\mu} \tag{2}$$

In Eq. (2), φ_u is the sliding friction angle, which is related to the stone content and internal structure of the shear band. When $\theta > \frac{\pi}{2}$, $\alpha = \theta - \frac{\pi}{2}$. When $\theta \le \frac{\pi}{2}$, $\alpha = \frac{\pi}{2} - \theta$. Substituting Eq. (2) into Eq. (1), we get

$$W_{\theta} = 2N\sin\alpha_0\tan\varphi_{\mu}a \tag{3}$$

The displacement work can be regarded as the work done by the external force on the center of gravity displacement trajectory. Then, the displacement work is

$$W_g = \int_{\frac{\pi}{2}+\alpha_0}^{\frac{\pi}{2}-\alpha_0} F ds \tag{4}$$

where ds is the tiny increment of particle displacement, and F is the component of shear force to displacement.

$$F = N\cos\alpha\cos\varphi_{\mu} \tag{5}$$

The trajectory of gravity center migration can be regarded as a part of the ellipse whose major half axis is R+a and the minor half axis is R+b. The displacement increment can be expressed as follows:

$$ds = \sqrt{(R+a)^2\cos^2\theta + (R+b)^2\sin^2\theta}\,d\theta \tag{6}$$

Substituting Eqs. (5) and (6) into Eq. (4), we obtain

$$W_g = N\tan\varphi_{\mu}\frac{AB\sinh(\sqrt{A^2-B^2}\sin\alpha_0) + \sqrt{A^2-B^2}\sin\alpha_0\sqrt{(A^2-B^2)\sin^2\alpha_0 + B^2}}{\sqrt{A^2-B^2}} \tag{7}$$

where A = R + a, and B = R + b. Therefore, the sum of occlusal work is

$$\begin{aligned} W_b &= W_{\theta} + W_g \\ &= N\tan\varphi_{\mu}\left[2\sin\alpha_0 a + \frac{AB\sinh(\sqrt{A^2-B^2}\sin\alpha_0) + \sqrt{A^2-B^2}\sin\alpha_0\sqrt{(A^2-B^2)\sin^2\alpha_0 + B^2}}{\sqrt{A^2-B^2}}\right] \end{aligned} \tag{8}$$

In addition, the work done by friction can be expressed as

$$W_t = \int_{\frac{\pi}{2}+\alpha_0}^{\frac{\pi}{2}-\alpha_0} f ds \tag{9}$$

W

Preprints (www.preprints.org) | NOT PEER-REVIEWED | Posted: 17 May 2021 doi:10.20944/preprints202105.0374.v1

Where ds is the relative displacement of sliding between particles, which can be approximately expressed as

$$ds = ds_1 + ds_2 = (R + \frac{a+b}{2})d\theta \tag{10}$$

According to the force balance in the Y-axis direction, it can be seen that when $\theta \le \frac{\pi}{2}$,

$$\frac{f\cos\alpha}{\tan\varphi_\mu} + f\sin\alpha = N \tag{11}$$

And when $\theta > \frac{\pi}{2}$,

$$\frac{f\cos\alpha}{\tan\varphi_\mu} - f\sin\alpha = N \tag{12}$$

Substituting Eqs. (10), (11), and (12) into Eq. (9), we get

$$W_t = N\left(\left(+\frac{a+b}{2}\right)\frac{1}{\sqrt{\tan^2\varphi_\mu + 1}}\ln\frac{[\tan\varphi_\mu\cos\alpha_0 + \sqrt{\tan^2\varphi_\mu + 1}(1+\sin\alpha_0) - \sin\alpha_0 - 1]}{[\tan\varphi_\mu\cos\alpha_0 - \sin\alpha_0 + \sqrt{\tan^2\varphi_\mu + 1}(-\sin\alpha_0 - 1) - 1]}\right.$$
$$\left.\frac{[\tan\varphi_\mu\cos\alpha_0 + \sin\alpha_0 + \sqrt{\tan^2\varphi_\mu + 1}(\sin\alpha_0 - 1) - 1]}{[\tan\varphi_\mu\cos\alpha_0 + \sqrt{\tan^2\varphi_\mu + 1}(1 - \sin\alpha_0) + \sin\alpha_0 - 1]}\right) \tag{13}$$

To quantitatively analyze the proportion of the work done by the bite force and the work done by friction under the change of the rock content, it is assumed that the angle α_0 between the contact surface and the horizontal plane at the initial position is 30°, the sliding friction angle between particles is 35°, R = 0.75 cm, a = 0.5 cm, b = 0.25 cm. According to the study by Wu et al. [33], the rock content can be expressed by a sine function in the bite force work. The proportion of work done by bite force and friction force under different rock content is calculated (Table 4). With the increase of rock content, the proportion of occlusal component increases gradually. When the rock content reaches 40%, the proportion of work done by bite force and friction force is close to 1:1. At this time, the contribution of bite force and friction force to the shear strength is equivalent, which is also why the shear strength of freezing–thawing interface is the largest under this rock content.

Table 4. Proportion of each component under different rock content.

Rock Content/%	W_b	W_t	W_b/W_t	Percentage of W_b (%)	Percentage of W_t (%)
0	0	0.984	0	0	100
10	0.281	0.984	0.286	22.2	77.8
20	0.552	0.984	0.561	35.9	64.1
30	0.080	0.984	0.821	45.1	54.9

Preprints (www.preprints.org) | NOT PEER-REVIEWED | Posted: 17 May 2021 doi:10.20944/preprints202105.0374.v1

35	0.927	0.984	0.942	48.5	51.5
40	1.038	0.984	1.055	51.3	48.7

4.2. Influence mechanism of rock content on shear strength of the interface

Based on the results of the direct shear test and the 3D topography scan of the shear surface, the mechanism of the shear strength change of the S-RM freezing–thawing interface under the change of the rock content can be analyzed (see Figure 9). During the direct shear test of the interface, part of the gravel are embedded in the frozen soil below the freezing–thawing interface. These gravel must be bypassed during the shearing process, and eventually an irregular shear surface is formed. Different rock content results in significant differences in the shear failure surface. The specific analysis is that when the rock content is low ($R \leq 30\%$), the actual shear surface fluctuates up and down along the freezing–thawing interface. Generally, the particles on the shear surface are broken, turned, and the shear surface formed is relatively flat, especially when the normal stress is low, the horizontal shear stress is not enough to cause the particles on the shear surface to break. The shear failure surface is more developed along the edge of the particles, which leads to the uneven shear surface, but the flatness is good in the local area of concave and convex, and finally the shear failure surface becomes wave-shaped failure. When the rock content is high ($R > 30\%$), the skeleton effect is more obvious. In addition to the continuous pushing and rotation of rocks in the part of the thawed soil and the lubrication of the ice layer, greater bonding resistance will be obtained at the freezing–thawing interface because some rocks are embedded in the part of the frozen soil. Finally, the flatness of the shear failure surface is poor, and a large range of pits can be seen on the failure surface, showing gnawing failure. The obvious change of failure mode is the reason for the threshold value of shear strength at $R = 30\%$.

The shear strength of cohesive soil is mainly provided by cohesion, while for S-RM with a large rock content, its shear strength is mainly provided by the friction angle. The friction angle increases with the increase in rock content. When the rock content is more than 10%, the compactness of the sample increases further, and the occlusion between particles begins playing a positive role rapidly, resulting in a sharp increase in cohesion. When the rock content is more than 35%, fine-grained soil is not enough to fill the skeleton formed by gravel, and the increase of occlusion is mainly reflected in the aggregation and overturning between gravel, which leads to the sharp increase in internal friction angle.

From the above analysis, it can be seen that when the rock content is low, gravel is suspended in the medium composed mainly of soil, and the distance between gravel is relatively large, and only a small amount of gravel in the frozen soil below the freezing–thawing interface can provide bite force. With the increase of rock content, the occlusion between particles near the interface increases obviously. The gravel in the frozen soil has stronger shear strength, and the interaction with the gravel in the melting soil can bear most of the shear force. In the process of gravel bite and rolling, the soil particles fill in the pores, and the gravel bite effect will be more obvious.

Preprints (www.preprints.org) | NOT PEER-REVIEWED | Posted: 17 May 2021 doi:10.20944/preprints202105.0374.v1

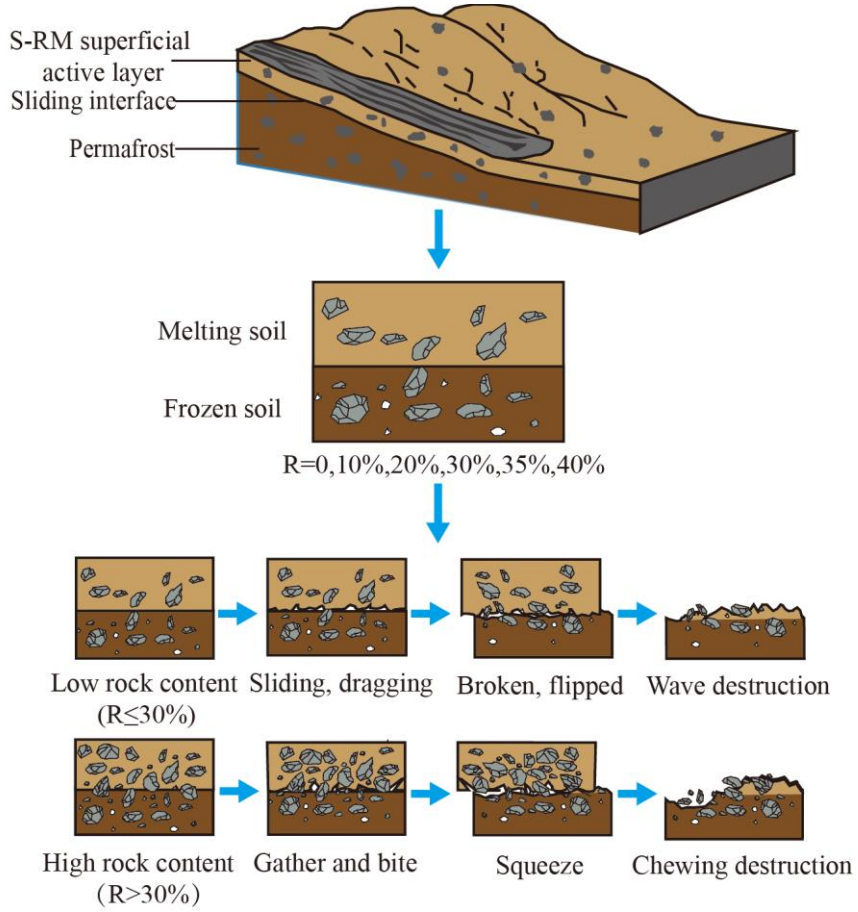

Figure 9. Instability mechanism diagram of soil-rock mixture slope in cold regions.

Conclusions

For the S-RM slope thawing process in permafrost regions, the influence of rock content on the shear strength of S-RM freezing–thawing interface was investigated through shear tests. The morphology of shear surface was obtained via 3D laser scanning. Based on the aforementioned test results and the shear band particle calculation model, the effect of rock content on the shear strength of S-RM freezing–thawing interface was analyzed. The main conclusions are as follows:

(1)When the normal stress was 50 and 100 kPa, the stress–strain curves of R ≤ 30% were of the strain-hardening type, and the stress–strain curves of R > 30% are strain softening type. With the increase in rock content, the stress–strain curves change from strain-hardening type to strain-softening type. When the normal stress is 150 and 200 KPa, the stress–strain curves show the characteristics of strain hardening and zigzag.

(2)With increasing rock content, the shear strength of the S-RM freezing–thawing interface increased. When the rock content was more than 30%, the shear strength of the interface increased rapidly. This is because when the rock content is large, the gravels in the thawed and frozen soils bite tightly, especially in the case of high stress, and the skeleton effect of the mixture is more obvious. As such, the threshold value of rock content on the interface strength is approximately 30%. The cohesion first decreased and then increased with increasing rock content, reaching the minimum when the rock content was 10% and then presenting a significant linear increase. The friction angle gradually increased with increasing rock content; when the rock content was 35%, it increased rapidly.

(3)Through the analysis and deduction of the calculation model of the S-RM freezing–thawing interface, it is believed that the increase in the occlusal force between the particles is the main reason for the increase in the shear strength of the interface with increasing rock content.

Preprints (www.preprints.org) | NOT PEER-REVIEWED | Posted: 17 May 2021 doi:10.20944/preprints202105.0374.v1

(4)During the shearing process, part of the rocks was embedded on the freezing–thawing interface and the shearing must bypass these rocks. Therefore, the real shear surface is not a smooth plane but a curved surface with some dislocation. In addition to the continuous pushing and rotation of rocks in the thawed soil and the lubrication of the ice layer, high bonding resistance was observed at the freezing–thawing interface because some rocks were embedded in the part of the frozen soil. When the rock content was low, the actual shear surface undulated like waves. When the rock content was high, the shear plane exhibited gnawing failure.

Author Contributions: Conceptualization, G.L.; investigation, T.H.; writing—original draft preparation, G.L.; writing—review and editing, T.H.; supervision, Z.L.; methodology, M.B. All authors have read and agree to the published version of the manuscript.

Funding: This work has been supported by the National Natural Science Foundation of China (grant No. 42071100).

Conflicts of Interest: The authors declare no conflict of interest.

References

1. Geertsema, M.; Clague, J.J.; Schwab, J.W.; Evans, S.G. An overview of recent large catastrophic landslides in northern British Columbia, Canada. *Eng. Geol.* **2006**, 83(1-3), 120-143. DOI: 10.1016/j.enggeo.2005.06.028
2. Tsesarsky, M.; Hazan, M.; Gal, E. Estimating the elastic moduli and isotropy of block in matrix (bim) rocks by computational homogenization. *Eng. Geol.* **2016,** 200, 58-65. DOI: 10.1016/j.enggeo.2015.12.003
3. Liu, S.Q.; Wang, H.L.; Xu, W.Y.; Chen, Z.C.; Xiang, Z.P.; Xie, W.C. Numerical Investigation of the Influence of Rock Characteristics on the Soil-Rock Mixture (S-RM) Slopes Stability. *KSCE. J. Civ. Eng.* **2020**, 24(11), 3247-3256. DOI: 10.1007/s12205-020-0034-1
4. Li, G.Y.; Yu, Q.H.; Ma, W.; Chen, Z.Y.; Mu, Y.H.; Guo, L.; Wang, F. Freeze–thaw properties and long-term thermal stability of the unprotected tower foundation soils in permafrost regions along the Qinghai-Tibet Power Transmission Line. *Cold. Reg. Sci. Technol.* **2016**, 121, 258-274. DOI: 10.1016/j.coldregions.2015.05.004
5. Niu, F.J.; Jing, L.; Lin, Z.J.; Fang, J.H.; Liu, M.H. Thaw-induced slope failures and stability analyses in permafrost regions of the Qinghai-Tibet Plateau, China. *Landslides* **2016**, 13(1), 55-65. DOI: 10.1007/s10346-014-0545-2
6. Wang, S.H., Ding, J.L.; Xu, J.; Ren, J.W.; Yang, Y.G. Shear strength behavior of coarse-grained saline soils after freeze-thaw. *KSCE. J. Civ. Eng.* **2019**, 23(6), 2437-2452. DOI: 10.1007/s12205-019-0197-9
7. Tang, L.Y.; Li, G.; Li, Z.; Jin, L.; Yang, G.S. Shear properties and pore structure characteristics of soil–rock mixture under freeze–thaw cycles. *B. Eng. Geol. Environ.* **2021**, 80(4), 3233-3249. DOI: 10.1007/s10064-021-02118-4
8. Bommer, C.; Fitze, P.; Schneider, H. Thaw-Consolidation Effects on the Stability of Alpine Talus Slopes in Permafrost. *Permafrost. Periglac.* **2012**, 23(4), 267-276, DOI: 10.1002/ppp.1751
9. Qi, C.Q.; Li, L.Y.; Wei, J.H.; Liu, J. Shear behavior of frozen rock-soil mixture. *Adv. Mater. Sci.Eng.* **2016**, DOI: 10.1155/2016/1646125
10. Hu, F.; Li, Z.Q.; Tian, Y.F.; Hu R.L. Failure Patterns and Morphological Soil–Rock Interface Characteristics of Frozen Soil–Rock Mixtures under Compression and Tension. *Appl. Sci.* **2021**, 11(1): 461.
11. Li, Z.Q.; Hu, F.; Qi, S.W.; Hu, R.L. Strain-softening failure mode after the post-peak as a unique mechanism of ruptures in a frozen soil-rock mixture. *Eng. Geol.* **2020**, 274, 105725, DOI: 10.1016/j.enggeo.2020.105725
12. Chen, H.; Guo, H.T.; Yuan, X.Q.; Chen, Y.T. Sun, C. Effect of Temperature on the Strength Characteristics of Unsaturated Silty Clay in Seasonal Frozen Region. *KSCE. J. Civ.l Eng.* **2020**, 24(9), 2610-2620, DOI: 10.1007/s12205-020-1974-1
13. Medley, E.; Lindquist, E.S. The engineering significance of the scale-independence of some Franciscan melanges in California. The 35th US rock mechanics symposium, Reno, NE, USA, June 5-7 1995.
14. Kalender, A.; Sonmez, H.; Medley, E.; Tunusluoglu, C.; Kasapoglu, K.E. An approach to predicting the overall strengths of unwelded bimrocks and bimsoils. *Eng. Geol.* **2014**, 183, 65-79, DOI: 10.1016/j.enggeo.2014.10.007
15. Avşar, E. Contribution of fractal dimension theory into the uniaxial compressive strength prediction of a volcanic welded bimrock. *B. Eng. Geol. Environ.* **2020**, 1-15, DOI: 10.1007/s10064-020-01778-y
16. Vallejo, L.E.; Mawby, R. Porosity influence on the shear strength of granular material–clay mixtures. *Eng. Geol.* **2000**, 58(2), 125-136, DOI: 10.1016/S0013-7952(00)00051-X
17. Simoni, A.; Houlsby, G.T. The direct shear strength and dilatancy of sand–gravel mixtures. *Geotech. Geol. Eng.* **2006**, 24(3), 523, DOI: 10.1007/s10706-004-5832-6
18. Xu, W.J.; Xu, Q.; Hu, R.L. Study on the shear strength of soil–rock mixture by large scale direct shear test. *Int. J. Rock. Mech. Min.* **2011**, 48(8), 1235-1247, DOI: 10.1016/j.ijrmms.2011.09.018
19. Coli, N.; Berry, P.; Boldini, D. In situ non-conventional shear tests for the mechanical characterisation of a bimrock. *Int. J. Rock. Mech. Min.* **2011**, 48(1), 95-102, DOI: 10.1016/j.ijrmms.2010.09.012

Preprints (www.preprints.org) | NOT PEER-REVIEWED | Posted: 17 May 2021 doi:10.20944/preprints202105.0374.v1

20. Wei, H.Z.; Xu, W.J.; Xu, X.F.; Meng, Q.S.; Wei, C.F. Mechanical Properties of Strongly Weathered Rock–Soil Mixtures with Different Rock Block Contents. *Int. J. Geomech.* **2018**, 18(5), 04018026, DOI: 10.1061/(ASCE)GM.1943-5622.0001131
21. McRoberts, E.C.; Morgenstern, N.R. The Stability of Thawing Slopes. *Can. Geotech. J.* 1974, 11(4), 447-469, DOI: 10.1139/t74-052
22. Niu, F.J.; Cheng, G.D.; Ni, W.K.; Jin, D.W. Engineering-related slope failure in permafrost regions of the Qinghai-Tibet Plateau. *Cold. Reg. Sci. Technol.* **2005**, 42(3), 215-225, DOI: 10.1016/j.coldregions.2005.02.002
23. Toloukian, A.R.; Sadeghi, J.; Zakeri, J.A. Large-scale direct shear tests on sand-contaminated ballast. *P. I. Civil. Eng-Geotec.* **2018,** 171(5), 451-46, DOI: 10.1680/jgeen.17.00107
24. Shi, S.; Zhang, F.; Feng, D.; Xu, X. Experimental investigation on shear characteristics of ice–frozen clay interface. *Cold Reg. Sci. Technol.* **2020**, 176, 103090, DOI: 10.1016/j.coldregions.2020.103090
25. Zeyl, D.P.V.; Penner, L.A.; Halim, R.A. A slope failure caused by drainage cutoff through the advancement of seasonal frost, Hudson Bay Lowland. *Landslides* **2013**, 10(3), 315-322, DOI: 10.1007/s10346-012-0377-x
26. Yu, W.B.; Liu, W.B.; Lai, Y.M.; Chen, L.; Yi, X. Nonlinear analysis of coupled temperature-seepage problem of warm oil pipe in permafrost regions of Northeast China. *Appl. Therm. Eng.* **2014**, 70(1), 988-995, DOI: 10.1016/j.applthermaleng.2014.06.028
27. Tang, L.Y.; Du, Y.; Liu, L.; Jin, L.; Yang, L.J.; Li, G.Y. Effect mechanism of unfrozen water on the frozen soil-structure interface during the freezing-thawing process. *Geomech. Eng.* **2020**, 22(3): 245-254, DOI: 10.12989/gae.2020.22.3.000
28. De, Guzman, E.M.B.; Stafford, D.; Alfaro, M.C.; Doré, G.; Arenson, L.U. Large-scale direct shear testing of compacted frozen soil under freezing and thawing conditions. *Cold. Reg. Sci. Technol.* **2018**, 151, 138-147, DOI: 10.1016/j.coldregions.2018.03.011
29. Cheng, Y.C.; Ge, Q.; He, F. Experimental Research on the critical depth of the slip surface of soil slope in the seasonal frozen area. *Rock. Soil. Mech.* **2010**, 31(4), 1042-1046, DOI: 10.16285/j.rsm.2010.04.028
30. Tang, L.Y.; Wang, X.; Qiu, P.Y.; Jin, L. Study on shear performance of soil-rock mixture at freezing-thawing interface in cold regions. *Rock. Soil. Mech.* **2020**, 41(10), 3225-3235, DOI: 10.16285/j.rsm.2019.2165 (In Chinese)
31. Lindquist, E.S.; Goodman, R.E. Strength and deformation properties of a physical model melange. 1st North American rock mechanics symposium, Austin, TX, USA, June 1-3 1994.
32. MWRPRC (Ministry of Water Resources of the People's Repoblic of China). *GB/T 50123-2019: Standard for geotechnical testing method*; China Planning Press: Beijing, China, 2019.
33. Wu, S.F.; Cai, H.; Wei, Y.Q.; Xiao, J.Z.; Yan, J. Shear mechanism and shear strength component characteristics of soil-stone mixtures. *Chin. J. Geotech. Eng.* **2019**, 41(S2), 230-234, DOI: 10.11779/CJGE2019S2058